

# Cylindrical Roller Bearing Hertz Line Contact Modeling and Analysis in Plane

Jakub Chmelař<sup>1</sup>

<sup>1</sup> ČVUT v Praze, Fakulta strojní, Ústav konstruování a částí strojů, Technická 4, 166 07 Praha 6, Česká republika

## Abstract

The article summarizes practical findings on area of elastic smooth bodies contact modeling in plane. Hertz contact theory is applied to calculate surface contact pressure and sub surface stress below center of contact. Detail graphical contour visualization of von Mises stress and principal shear stress magnitude and plane direction is modeled with FEM. The results show very complex material loading, which continuously changes it's states during roller element pass.

**Keywords:** STČ; Contact modeling, Hertz contact, Sub-surface stress

## 1. Introduction

Bearings became one of the most important components of machines with rotating parts during the last century. They allow relative rotational motion of two parts with minimal energy loss. Due to they critical importance in reliability of machines, they are subject of research in area of fatigue and reliability prediction. This article is focused on methods of bearing race contact load modeling by means of analytical description and FEM approach that forms basis for further research.

## 2. Bearing analysis

### 2.1. Standards

Current standards used for general evaluation and sizing of bearings provide very efficient tools for quick analysis and prediction of bearing life.

The essential standard ČSN ISO 281 [1] provides users with very simple way of bearing life prediction that could be calculated with standard hand calculator. External bearing load, usually combination of acting radial and axial force is recalculated to equivalent load -P based on bearing internal geometry. The bearing internal geometry and material information are involved in parameter called basic dynamical capacity -C and easy to remember parameter load – life exponent, that express relationship between life and applied load. The value varies with contact nature – point or line. [2]

$$L_{10} = \left(\frac{C}{P}\right)^n \quad (1)$$

This simple method is in the standard ČSN ISO 281 [1] extended to cover influences of lubrication type, lubricant cleanliness, and even quality and development of lubrication layer. Mentioned factors are expressed by  $a_1$  and  $a_{iso}$  values in the standard and modify the basic rating life and provide user with even more accurate life estimation for given conditions.

$$L_{nm} = a_1 a_{ISO} \left(\frac{C}{P}\right)^n \quad (2)$$

Limits of this method are obvious. It does not allow detailed bearing load inputs and neither analysis involving bearing internal geometry.

More accurate method is published in standard ISO / TS 16 281 [3] that uses a mathematical model of bearing including internal geometry. It can therefore provide engineer with much detailed information about inner load distribution. Unlike ČSN ISO 281 [1] that only covers normal loading forces (radial and axial), ISO/TS 16281 [3] works also with tilting moment that is usually introduced when kinematical limits of bearing are exceeded. It also works with parameters such as number of rolling elements, bearing inner clearance, manufacturing and tolerance class when it calculates bearing internal load distribution.

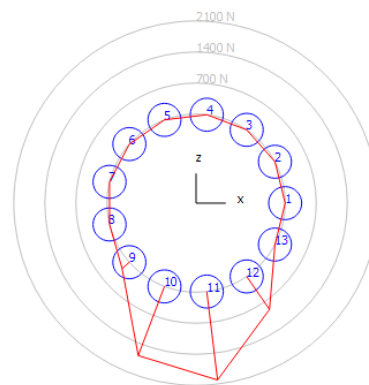


**Fig. 1.** Roller element load distribution calculated according to ISO/TS 16 281. Loading is in negative z axis, direction

Bearing life calculation is based on similar theory as in case of ISO 281:2007, but it is calculated with respect to actual inner load distribution.

\* Kontakt na autora: Jakub.Chmelař@fs.cvut.cz

Use of bearing calculation according to ISO/TS 16281 [3] requires its implementation in computational software. On the market, for example MESYS and KISSsoft are available.

## 2.2. Advanced analysis concept

The knowledge of bearing inner load distribution is a key to advanced analysis of material response. ISO/TS 16281 [3] provides unique tools for detailed internal load analysis. The limits are in the evaluation that is based on Lundberg and Palmgren's [4] theory where the stress field below contact is expressed by derived analytical equations. These are sufficient for engineering purposes, but limiting when advanced research is requested.

Possible way of advancement was conducted. Standard ISO/TS 16281 [3] was used for obtaining bearing inner load distribution and contact was modeled by means of FEM method, where appropriate model of contact was assembled and solved. This opens new possibilities of contact modeling, analysis and assessment.

## 3. Analytical Contact Assessment

### 3.1. Hertz line contact analytical solution

First theoretical explanation on elastic contact of two bodies was presented by Hertz at the end of 19th century. He made an assumption that in contact of two smooth bodies the contact region is a small with elliptical shape. That allowed him separating stresses induced by contact from general stresses that arises inside of both contact bodies as response to load. [5]

When bearing contacts are discussed there could be distinguished three types of Hertzian contacts, namely: (i) Elliptical contact – typical for ball bearings (ii) Line contact – typical for roller bearings. (iii) Point contact is not in bearing technology common, since all standard bearings have their races curved and therefore it results in elliptical contact area shape.

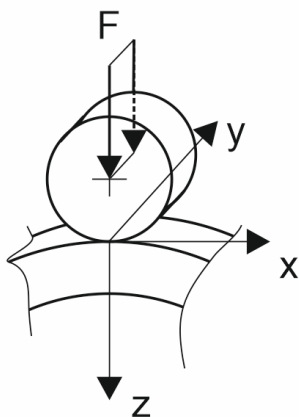


Fig. 2. Line contact coordinate system

Further investigation was limited to line contact of two cylindrical bodies. (that is based on general elliptical contact, but slightly simplified). Geometrical parameters

are viewed on Fig. 2 and Fig. 3. The length of contact  $l$  is considered to be infinite, loading is evaluated per unit of length and width of contact is denoted as  $2a$  where  $a$  is considered to be a length of ellipse semiaxis.

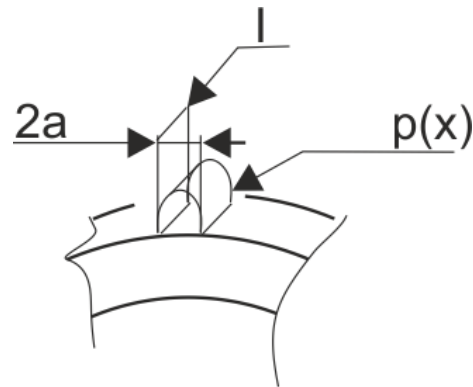


Fig. 3. Line contact description parameters

Presented theory is based on following assumptions, that if held, it provides reasonable results:

- Length of bodies is much greater than contact area width:  $l \gg 2a$
- Width of contact area is small comparing to radii of contact bodies:  $2a \ll R_i$
- Bodies are smooth, no friction is considered,  $\mu=0$
- Deformation of bodies are small compared to its size
- Elastic material behaviour is considered

From derivation included in [5] there are established substitutions – see (3) that is a sum of relative curvatures of both non-conforming bodies.

$$\frac{1}{R} = \frac{1}{R_1} + \frac{1}{R_2} \quad (3)$$

An effective Young's modulus – see (4)

$$\frac{1}{E^*} = \frac{1-\nu_1}{E_1} + \frac{1-\nu_2}{E_2} \quad (4)$$

It could be estimated that acting force per unit length will result in contact area with semiaxis width (5).

$$a^2 = \frac{4FR}{\pi E^*} \quad (5)$$

The pressure distribution that is assumed to have an elliptical shape, shall be calculated with respect to coordinate  $x$  according to Fig. 2, Fig. 3 and (6).

$$p(x) = \frac{2F}{\pi a^2} (a^2 - x^2)^{1/2} \quad (6)$$

Maximal pressure  $p_0$  of line contact is then calculated according to (7).

$$p_0 = \frac{2P}{\pi a} = \sqrt{\frac{FE^*}{\pi R}} \quad (7)$$

### 3.2. Plane strain assumption

Contact of two bodies is treated as plane strain, loading is assumed to act in XZ plane and length of bodies is infinite. The load does not change with y coordinate. For such, we assume following conditions (8)-(10):

$$\varepsilon_y = \gamma_{xy} = \gamma_{yz} = 0 \quad (8)$$

Out-of plane shear stress is not considered

$$\tau_{xy} = \tau_{yz} = 0 \quad (9)$$

Even though we consider plane strain conditions, there still occurs a transverse stress component

$$\sigma_y = \nu(\sigma_x + \sigma_z) \quad (10)$$

### 3.3. Subsurface stress development

Surface contact stress induced by contact of both elastic bodies results in stress response in the material below surface. There were derived analytical equations describing the stress field [5]. Those if simplified for contact centre, result in following equations of principal stress development in XZ plane [6]

$$\sigma_1 = \sigma_x = -p_0 \left[ \left( 2 - \left( \frac{z^2}{a^2} + 1 \right)^{-1} \right) \sqrt{\left( \frac{z^2}{a^2} + 1 \right)} - 2 \left| \frac{z}{a} \right| \right] \quad (11)$$

$$\sigma_2 = \sigma_y = -2p_0 \left[ \sqrt{\left( \frac{z^2}{a^2} + 1 \right)} - \left| \frac{z}{a} \right| \right] \quad (12)$$

$$\sigma_3 = \sigma_z = -p_0 \left[ \sqrt{\left( \frac{z^2}{a^2} + 1 \right)} \right]^{-1} \quad (13)$$

### 3.4. Stress evaluation

Stress effect evaluation could be performed in the first place according to hypotheses allowing comparison multiaxial stress state to known material data obtained from uniaxial experimental measurements.

### 3.5. Tresca Maximal shear stress

Principal shear stress in XZ plane, often called as Tresca, predicts that the yield of material shall occur if maximal shear stress exceeds the value of maximal shear stress from uniaxial tensile test. Maximal shear stress in plane is thus calculated as half of difference between two principle stress components.

$$\tau_2 = \tau_{XZ} = \tau_{Tresca} = \left| \frac{\sigma_1 - \sigma_3}{2} \right| \geq \frac{1}{2} \sigma_Y \quad (14)$$

#### 3.2.2 Von Mises criterion

When employed criterion of distortional strain energy the von Mises's equivalent stress would be calculated from principal stresses and first yield would in this material appear if strain distortional energy of multi-axial stress state exceeds the strain energy at yield of uniaxial tensile test.

$$\sigma_{VM} = \sqrt{\frac{1}{2} [(\sigma_1 - \sigma_2)^2 + (\sigma_1 - \sigma_3)^2 + (\sigma_2 - \sigma_3)^2]} \geq \sigma_Y \quad (15)$$

And thus it could be proven, that shear stress known as octahedral would be calculated:

$$\tau_{oct} = \frac{1}{3} \sqrt{[(\sigma_1 - \sigma_2)^2 + (\sigma_1 - \sigma_3)^2 + (\sigma_2 - \sigma_3)^2]} \quad (16)$$

Both criterion are widely used for stress assessment of multi-axial stress states and both very well fits experimental data for most ductile materials. The difference between either is that Tresca predicts the material yield in slightly lower stresses compared to von Mises octahedral stress. [7]

### 3.5.1. Quick stress estimation

Substituting (11) – (13) to (14) and (15) it is possible to obtain values of maximal shear stress and von Mises stress together with magnitude of peaks position. These easy to remember values are summarized in Table 2.

Table 2. Quick stress estimation.[2]

Criterion	Estimation
Max. shear stress value	$0.3 \cdot p_0$
Max. shear stress depth	$0.78 \cdot a$
Von Mises stress max. value	$0.56 \cdot p_0$
Max. Von Mises stress depth	$0.7 \cdot a$

## 4. FEM contact modelling

### 4.1. Assembly

The problem consists of two planar bodies – inner race and roller forced to mutual contact by applied boundary conditions. It is assumed quasi-static load case, so dynamic and cyclic loading is not considered. Applied boundary conditions are viewed on Fig. 4 The geometry of roller is constrained to Reference Point (RP1) where only motion in vertical axis is allowed. Inner diameter of race is constrained to second Reference Point (RP2) that all degrees of freedom are locked providing the inner race with absolutely stiff support simulating a shaft.

Geometry of bearing NU 206 was obtained from database of KISSsoft software and important values are viewed in table below

Table 3. Bearing geometry information.

	d	D	B	Di	Lwe	Dw
NU 206	30	62	15	37,5	10	9

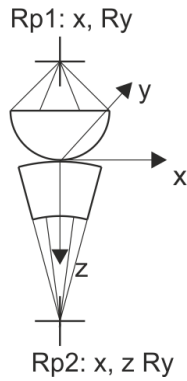


Fig. 4. FEM model in Abaqus. Constrained Degrees of freedom listed next to Reference point designation

## 4.2. Material

For both bodies there was used materials with elastic properties according standard bearing steel 100Cr6 Q+T. No plastic deformation was for this analysis considered, since it will be subject of further research.

Table 4. Bearing material typical propeties. [8]

Material	E	$\nu$	$\sigma_y$	HRC
100Cr6	2.1e5	0.3	2000	60

## 4.3. Contact propeties

Contact faces were assigned to be in mutual contact. Master surface was assigned to roller and slave to the race. Advanced Surface-to-Surface discretization was used. Due to very limited amount of sliding between both bodies small sliding contact formulation could be used [9]. The contact between both bodies was considered as frictionless in tangential direction and hard contact in normal direction was used.

## 4.4. Mesh

The problem is modelled as planar thus planar quad elements with mid-side nodes and reduced integration scheme – Abaqus designation: CPE8R was used. The element belongs to Plane Strain Element family and is purposed for general contact application where no complex changing conditions are assumed [9].

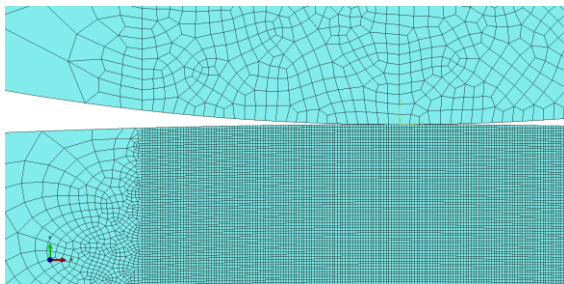


Fig. 5. Detail of mesh in area of contact

As viewed in Fig. 5 density of mesh is increasing in area of contact and becomes coarse in peripheral areas. The mesh of race is intended to be finer than mesh of roller because development of subsurface stress will in that area be inspected.

Global element size was assigned to 0.1 mm and the mesh is generated as free, consisting of quad elements. Contact line and region in neighbourhood of contact on the other side are meshed with structured mesh and element size 0.005 mm that would describe the region with enough detail to catch the stress field accurately Very fast transition of element size viewed on picture above does not affect the solution, because of main interest is region in the centre of fine meshed area. Fast transition only might cause instability of numerical solution.

## 5. Results

### 5.1. Hertz Contact Pressure Distribution

Comparison of contact stress solutions is viewed in Fig. 6. FEM solution accurately follows analytical stress development according to (6) except minor Hertz contact pressure solution error at peripherals of contact – grey dotted line in Fig. 6. Hertz contact pressure analytical and FEM solution comparison. Contact pressure 1620MPa. This error (computed by Abaqus and having same unit as parental [MPa], reaches up to 100 MPa) arises due to low contact pressure at peripherals and discretization of contact by elements. It will not influence main solution results.

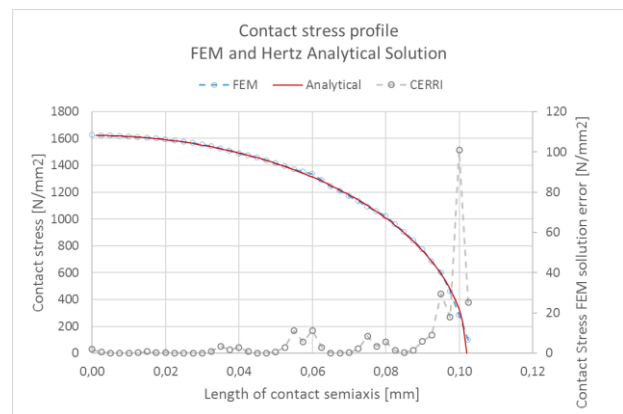


Fig. 6. Hertz contact pressure analytical and FEM solution comparison. Contact pressure 1620MPa

### 5.2. Sub surface stress development

Analytical solution provides equations for obtaining development of principal stresses below centre of contact – (11) – (13). These are used to calculate principal shear stress according to Tresca (14) that is thought to be responsible for fatigue damage resulting from local plasticity below surface [2] and therefore is generally [2], [10] used for evaluation of stress effect on the structure

Development of principal stresses ( $S_x$ ,  $S_z$ ,  $S_{xz}$ ) below centre of contact is presented in Fig. 7. Maximal value is  $\tau_{max} = 503,9 \text{ N/mm}^2$  is reached in depth  $z = 0,079 \text{ mm}$

below contact surface. FEM solution accurately follows analytical.

Comparing curves of Tresca and von Mises stress respectively in Fig. 7, we can see that there is visible difference in area close to contact surface. Difference is driven by out-of plane stress component that is involved in von Mises stress calculation and missing in in-plane Tresca shear stress solution.

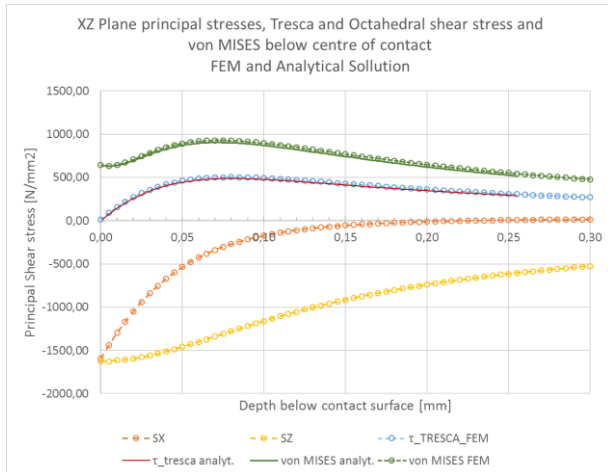


Fig. 7. Sub-surface Maximal Shear, Octahedral and von Mises Stress contours for contact pressure 1620 Mpa

Tresca Shear stress contours are viewed in Fig. 8. Where is clear evidence of maximal stress value below surface. The differences between lower and upper stress „structures“ is only due to different mesh quality for roller and race.

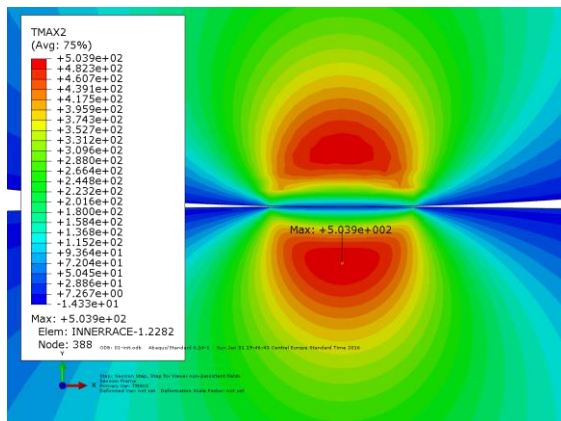


Fig. 8. Sub-surface Maximal Shear, Octahedral and von Mises Stress contours for contact pressure 1620 MPa

### 5.3. Principal stress and strain planes direction

When rolling element passes observed virtual point on contact surface, it could be viewed following development of maximal shear stress magnitude and angle of its acting plane in depth  $z = 0.08\text{mm}$  below surface Fig. 9. It is where maximal shear stress reaches its maximal values as specified in Table 2. It is obvious in that the angle of principal shear stress plane flips rapidly below the contact centre point. Principal

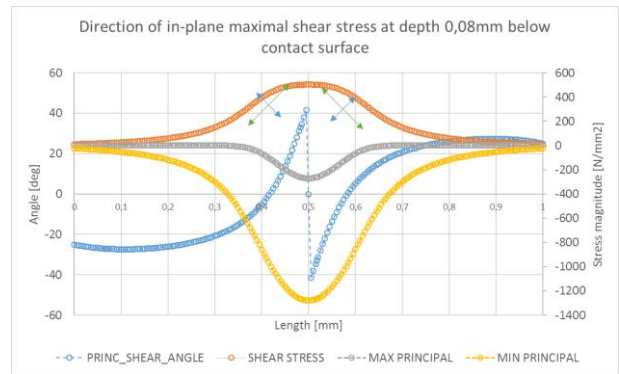


Fig. 9. Direction of Maximal Shear Stress plane, Magnitude of maximal shear stress and inplane principal stresses at depth  $z=0,08\text{mm}$  below contact of surface

Better overview of maximal shear stress plane direction can provide us Fig. 10. Very fast direction change below contact is aparent through the depth of material.

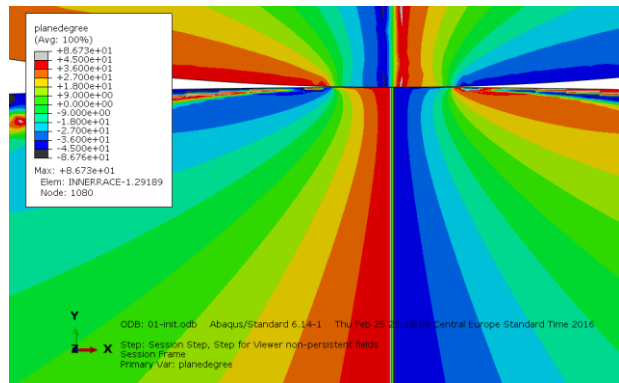


Fig. 10. Max. shear stress plane directions. Visualisation limited to  $\pm 45^\circ$

Fig. 11 shows direction and relative sizes of principal in-plane strain components and thus material deformation. The deformation is almost exclusively multi-directional. In vertical direction the there is compressive loading of material, but in horizontal direction, the material is mostly loaded in tension. There is a small region, just below the surface, where even material loading parallel to race is also compressive.

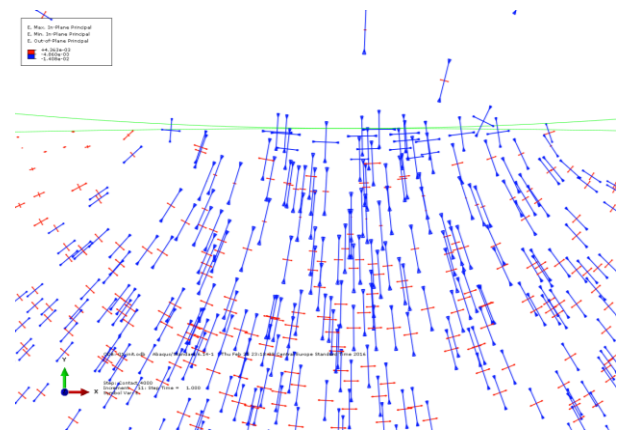


Fig. 11. In-Plane principal strain tensor visualization

#### 5.4. Known limitations

Proposed solution was limited to elastic material behaviour and smooth frictionless surface contact, that can in real working conditions be reached only under certain circumstances. Presented Hertz contact solution, in connection with bearing technology, is only valid if the lubrication layer between both contact surfaces is fully developed into Elastohydrodynamic (EHL) [11] state that prevents surface roughness asperities contact.

The elastic solution can influence and predict material sub/surface stress development, mainly in area of maximal shear stress or von Mises stress respectively, where values of material yield could be exceeded and some plastization can occur.

Solution also neglect the stress at the ends of roller, where spation attitude should be applied.

### 6. Discussion

Hertz analytical solution provides very efficient tools and method to quick analysis of sub-surface stress development, although FEM allow performing deep analysis, that provides better understanding of problem. Following results were obtained.

Maximal shear stress **Fig. 7** in centre of contact is located below contact surface in depth, that according to Hertz solution could be easily estimated. The value was verified by FEM. Shear stress contours are viewed in **Fig. 8**. This max shear stress is driven by difference of in-plane principal stresses.

Maximal shear stress acting plane is near centre of contact and changes rapidly direction from  $+45^\circ$  to  $-45^\circ$  during roller pass. It is graphically represented on **Fig. 9**, where development of in-plane principal stresses in depth 0.08mm below contact surface is viewed. During the roller pass, every point of material is stressed un proportionally in all three axes. Good overview of the material loading complexity is in **Fig. 11**. Where is the visualization of principal strain tensor. There could be distinguished a small region below the contact where material loading is only compressive and thus it should have protective effect on material.

Peak of von Mises stress is located slightly deeper below contact surface **Fig. 7**. Because of out of plane stress solution influence, there is obvious surface stress magnitude, which although has compressive character.

#### Symbols

a	Contact half-width (mm)
$a_1$	Bearing life modification factor - reliability
$a_{iso}$	Bearing life modification factor - lubrication
B	Bearing width (mm)
C	Dynamic capacity (N)
d	Bearing hole diameter (mm)
D	External bearing diameter (mm)
$D_i$	Bearing Inner race diameter (mm)
$D_w$	Roller diameter (mm)
$E_i$	Elasticity modulus ( $i=1$ or $2$ ) ( $N/mm^2$ )
$E^*$	Elasticity modulus substitution ( $N/mm^2$ )

F	Load acting on contact body (N)
L10	Basic bearing rating life (cycles)
$L_{we}$	Roller active length (mm)
l	Contact length (mm)
n	Bearing Load-Life exponent
P	Equivalent bearing load (N)
$p_0$	Maximal contact pressure
$p(x)$	Contact load along x axis (MPa)
$R_i$	Contact body radius ( $i=1$ or $2$ ) (mm)
x	Coordinate on X axis (mm)
z	Coordinate on Z axis (mm)
$\mu$	Friction coefficient
$\nu$	Poissons constant
$\pi$	Ludolf's number (3,141592654)
$\epsilon_i$	Strain ( $i=x, y, z$ )
$\gamma_{ii}$	Strain angle ( $i=x, y, z$ )
$\sigma_i$	Normal stress ( $i=x, y, z$ for orthogonal, $i=1,2,3$ for principal stresses)
$\tau_{ii}$	Shear stress ( $i=x, y, z$ for orthogonal, $i=1,2,3$ for principal stresses)
$\sigma_Y$	Material Yield stress
$\sigma_{VM}$	Stress according to von Mises criterion
$\tau_{Tresca}$	Shear stress according to Tresca
$\tau_{Oct}$	Octahedral Shear stress

### Literature

- [1] ČSN ISO 281, Valivá ložiska - Dynamická únosnost a trvanlivost. .
- [2] T. A. Harris and M. N. Kotzalas, Essential concepts of bearing technology. CRC press, 2006.
- [3] ISO/TS 16281:2008, Rolling bearings — Methods for calculating the modified reference rating life for universally loaded bearings. .
- [4] ISO/TR 1281-1:2008, Explanatory notes on ISO 281 — Part 1: Basic dynamic load rating and basic rating life. .
- [5] K. L. Johnson, Contact Mechanics, Ninth. Cambridge University Press, 2003.
- [6] E. Bamberg, 'Contact Stresses and Deformations', University of UTAH.
- [7] J. F. Doyle, Modern experimental stress analysis: completing the solution of partially specified problems. Hoboken, NJ: Wiley, 2004.
- [8] 'Steels for Bearing production from OVAKO'. Ovako.
- [9] 'Abaqus 6.14 Online Documentation'. © Dassault Systèmes, 2014, 23-Apr-2014.
- [10] E. V. Zaretsky, 'Rolling Bearing Life Prediction, Theory, and Application', NASA, John H. Glenn Research Center, Lewis Field, Cleveland, Ohio, Technical Paper NASA/TP-2013-215305, 2013.
- [11] H. Spikes, 'Basics of EHL for practical application', Lubr. Sci., vol. 27, pp. 45–67, 2015.